Research Article Vol. 4, No. 11 / November 2017 / Optica 1358

Solid-state-biased coherent detection of ultra-broadband terahertz pulses

Alessandro Tomasino,[1,4] Anna Mazhorova,[1] Matteo Clerici,[2] Marco Peccianti,[3] Sze-Phing Ho,[1,5] Yoann Jestin,[1] Alessia Pasquazi,[3] Andrey Markov,[1] Xin Jin,[1] Riccardo Piccoli,[1] Sebastien Delprat,[1] Mohamed Chaker,[1] Alessandro Busacca,[4] Jalil Ali,[5] Luca Razzari,[1] and Roberto Morandotti[1,6,7,*]

[1]INRS-EMT, 1650 Boulevard Lionel-Boulet, Varennes, Québec J3X 1S2, Canada
[2]School of Engineering, University of Glasgow, Glasgow G12 8LT, UK
[3]Department of Physics and Astronomy, University of Sussex, Brighton BN1 9RH, UK
[4]DEIM, University of Palermo, Viale delle Science, Palermo 90128, Italy
[5]Laser Centre, Ibnu Sina ISIR, UTM, 81310 UTM Skudai, Malaysia
[6]National Research University of Information Technologies, Mechanics and Optics, 199034 St. Petersburg, Russia
[7]Institute of Fundamental and Frontier Sciences, University of Electronic Science and Technology of China, Chengdu, 610054 Sichuan, China
*Corresponding author: morandotti@emt.inrs.ca

Received 25 September 2017; accepted 27 September 2017 (Doc. ID 307893); published 31 October 2017

Significant progress in nonlinear and ultrafast optics has recently opened new and exciting opportunities for terahertz (THz) science and technology, which require the development of reliable THz sources, detectors, and supporting devices. In this work, we demonstrate the first solid-state technique for the coherent detection of ultra-broadband THz pulses (0.1–10 THz), relying on the electric-field-induced second-harmonic generation in a thin layer of ultraviolet fused silica. The proposed CMOS-compatible devices, which can be realized with standard microfabrication techniques, allow us to perform ultra-broadband detection with a high dynamic range by employing probe laser powers and bias voltages much lower than those used in gas-based techniques. Eventually, this may pave the way for the use of high-repetition-rate ultrafast lasers and commercially available electronics for the coherent detection of ultrashort THz pulses.

OCIS codes: (040.2235) Far infrared or terahertz; (190.4380) Nonlinear optics, four-wave mixing; (190.4360) Nonlinear optics, devices; (140.7090) Ultrafast lasers; (040.6070) Solid state detectors.
https://doi.org/10.1364/OPTICA.4.001358

1. INTRODUCTION

During the past decades, there has been a growing interest in the terahertz (THz) spectral range, situated between the microwave and optical domains [1]. Terahertz radiation enables a variety of applications and provides opportunities to different research areas such as imaging, spectroscopy, and telecommunications [1–4]. Many of these achievements are related to the capability of emitting wideband THz pulses and to the possibility of reconstructing their exact field evolution in time. Within this context, many efforts have been devoted to achieving high-efficiency, cost-effective THz sources and detectors that are able to operate at room temperature over an ultra-broadband frequency range (0.1–10 THz). Nowadays, research labs and companies own a wide portfolio of THz-time domain spectroscopy (THz-TDS) systems, performing field-resolved experiments with bandwidths up to 7 THz [5–7]. Among these, the most widespread detection techniques rely either on the use of photoconductive antennas [8,9] or electro-optic sampling (EOS) in quadratic media (such as ZnTe and GaP crystals) [10,11]. However, the goal to coherently detect (i.e., both in phase and amplitude) ultra-broadband THz pulses, without introducing unwanted distortions, cannot be easily accomplished with either of these two methods. This is because they inherently suffer from detrimental effects related to long free-carrier lifetimes and phonon resonances [5]. To overcome these problems, a class of detection techniques relying on electric-field-induced second-harmonic (EFISH) generation [12] has been introduced. In such a process, an intense static electric field breaks the symmetry of a centrosymmetric (Kerr, $\chi^{(3)}$) medium (such as air or silica), inducing an electric-field-driven quadratic nonlinearity. Likewise, a THz field can be regarded as static over the duration of an ultrashort optical probe pulse, thus leading to its frequency doubling [12,13]. Furthermore, it has been shown that coherent detection schemes can be obtained by mixing the EFISH signal generated in air with an additional optical local oscillator at the same central frequency [14–16]. Among them, the most widely diffused approach is the air-biased coherent detection (ABCD) [16,17], where the optical local oscillator is obtained from an external static electric field E_{bias},

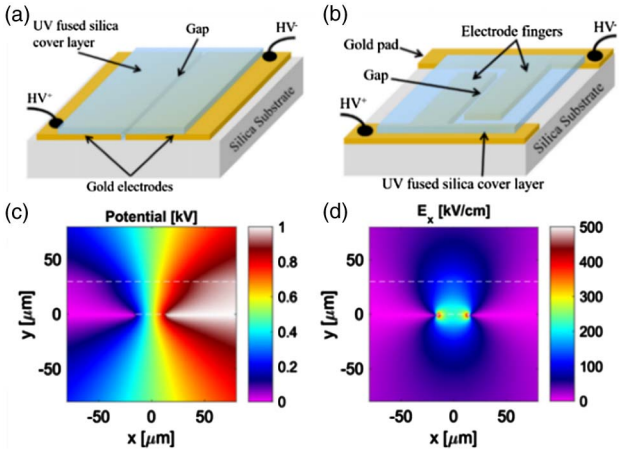

Fig. 1. Schematics of the two types of SSBCD devices and simulations of the bias field distribution. (a) Micro-slit, featuring a 30-μm-large silica gap and two large gold electrodes, and (b) subwavelength slits, featuring a few-micrometer silica gap and two electrode fingers. Finite difference method simulations showing (c) the static potential distribution and (d) the corresponding static electric field around the 30-μm-wide slit for a bias voltage of 1 kV (dashed white lines indicate the silica–air interface).

which biases the interaction between the THz and probe beams. The total intensity of the second-harmonic (SH) beam is expressed by the following equation [16]:

$$I_{\mathrm{SH}}^{\mathrm{total}} \propto (\chi^{(3)} I_{\omega})^2 [(E_{\mathrm{THz}})^2 + (E_{\mathrm{bias}})^2 \pm 2 E_{\mathrm{THz}} E_{\mathrm{bias}}], \quad (1)$$

where $\chi^{(3)}$ is the third-order susceptibility of the nonlinear medium, I_{ω} the optical probe intensity, and E_{THz} the THz electric field. Here, the double sign in the cross term depends on the relative phase between E_{THz} and E_{bias}. By performing the acquisition through a lock-in amplifier synchronized to the modulation frequency of the bias voltage, only the cross term in Eq. (1) is recorded, which scales linearly with the THz electric field. Due to the very low dispersion of air, ABCD allows us to record THz pulses with bandwidths exceeding 10 THz (ultra-broadband), although it requires kilovolt (kV) bias sources and tens of microjoule (μJ) probe energies. In this paper, we report on the novel implementation of a biased coherent detection technique that exploits the high nonlinearity [18] (effective $\chi^{(3)} \sim 2.2 \times 10^{-22}$ m^2/V^2) and dielectric strength (>200 kV/mm) of thin films of pure silica deposited via CMOS-compatible techniques [19]. Specifically, we take advantage of the THz–near-infrared nonlinear interaction in a thin layer of ultraviolet (UV) fused (i.e., pure) silica, biased by a pair of gold electrodes; see Figs. 1(a) and 1(b). Henceforth, we name the proposed technique solid-state-biased coherent detection (SSBCD). Our method allows the characterization of THz pulses with bandwidths as wide as those measured via standard ABCD, with the additional advantage of requiring three orders of magnitude lower optical probe energy and ten times lower bias voltage in similar experimental conditions.

2. EXPERIMENTAL RESULTS AND DISCUSSION

We report on our investigations on two generations of SSBCD detectors. The first-generation prototype, shown in Fig. 1(a), was used as proof of concept, whereas the second, in Fig. 1(b), was employed to investigate the effect of the main design parameters on the operating mechanism. The microfabrication process employed to fabricate the first-generation devices consists of the sputtering deposition of a 100-nm-thick layer of gold on a 2-mm-thick UV fused silica substrate. The gold layer is sandwiched between two 30-nm-thick layers of chromium to ensure the proper adherence of the gold pads to the silica. The electrodes are then defined by direct-write laser lithography and wet etching techniques to form a 30-μm-wide gap between them. Subsequently, a 30-μm-thick layer of fused silica is deposited over part of the electrodes—thus also filling the slit gap—via the plasma-enhanced chemical vapor deposition technique. For the second-generation batch, the electrode fingers and the narrower gaps are still patterned using direct-write laser lithography, followed by a standard lift-off process.

The Cr/Au/Cr layers (of 15 nm/90 nm/15 nm, respectively), are deposited by e-beam evaporation. Note that the cover silica layer is only 3-μm-thick in this case. Three devices, featured by 2-mm-long, 10-μm-wide fingers and different gap sizes of 3, 4, and 5 μm, respectively, have been fabricated (see Supplement 1). A fourth sample, featured by 100-μm-wide fingers and a 3-μm gap has also been realized. Numerical simulations, presented in Figs. 1(c) and 1(d), show that the bias electric field is confined inside the silica. The cover layer on top of the electrodes avoids unwanted discharging in air. The performance of our detector has been characterized by means of a THz-TDS setup (Fig. 2) operating in the ultra-broadband regime [16] and pumped by a Ti:Sapphire regenerative amplifier (800 nm, 150 fs, 2.2 mJ, 1 kHz); see Supplement 1. We employed a two-color plasma source emitting THz pulses featured by a 10-THz bandwidth. We estimated a THz peak electric field of 50 kV/cm at the device position, measuring the THz pulse energy with a pyroelectric detector, the beam profile with a THz camera, and the THz waveform via standard ABCD [20]. The latter was implemented by placing two tip-shaped electrodes at the focus position of the last parabolic mirror. The air gap between the tips was around 1.5 mm, and the probe power was fixed at 100 mW. We biased

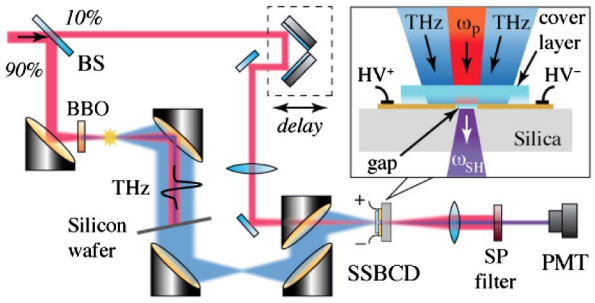

Fig. 2. Sketch of the ultra-broadband THz-TDS setup. An ultrashort optical pulse is spit into pump and probe beams by means of a 90/10 beam splitter (BS). The pump is focused with its second harmonic (SH), achieved through a beta barium borate (BBO) crystal, to generate a two-color plasma emitting THz pulses. A series of 90° off-axis parabolic mirrors handle the THz beam, whereas a high-resistivity 0.5-mm-thick silicon wafer blocks the residual SH and infrared beams. THz radiation is then focused along with the probe beam into the SSBCD device, placed on the focus of the last parabolic mirror. A shortpass (SP) filter rejects the residual probe pulse, while a photomultiplier tube (PMT) acquires the generated SH beam. The inset shows how THz, probe, and bias electric fields interplay to generate the SH beam.

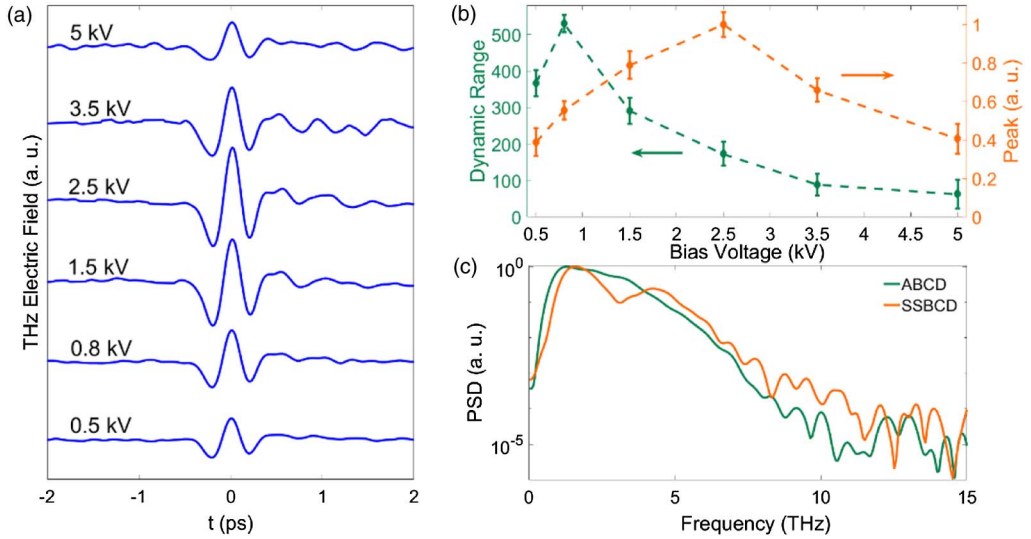

Fig. 3. (a) THz electric field transients recorded via the 30-μm-wide slit as a function of the bias voltage. For clarity, the curves are shifted along the *y* axis. (b) Corresponding dynamic range (dashed green line) and peak signal (dashed orange line) trends as a function of the bias voltage. (c) Power Spectral Density (PSD) evaluated via fast Fourier transform (FFT) of the THz waveform at 800 V: comparison between standard ABCD technique (solid orange line) and detection via the micro-slit (SSBCD) device (solid green line).

the interaction with a 2.5 kV square wave voltage at a modulation frequency of 500 Hz, while the averaging time on the lock-in amplifier was set to 100 ms. Starting with the first-generation device, we determined the SSBCD amplitude response and the corresponding dynamic range (DR, defined as reported in Naftaly and Dudley [21]) along with the THz peak electric field as a function of the bias voltage. We highlight that we fixed the probe power at 100 μW for all the SSBCD measurements while keeping the same focusing condition of the ABCD case. Figure 3(a) shows that the THz waveforms are not affected by the increasing bias voltage, thus maintaining the same shape. However, the measured signal is amplified only for a certain range of bias values, reaching its maximum for a voltage of 2.5 kV. Higher voltages result in a degradation of the signal [Fig. 3(b), peak trend]. This is most likely due to pre-breakdown phenomena occurring inside the silica for very high static electric fields (either carrier injections through the metal–dielectric interface or stress applied to the silicon–oxygen bond [22]) distorting the field distribution between the electrodes and eventually lowering the detection efficiency. In order to evaluate the performance of our device, we studied the trend of the DR as a function of the bias voltage.

The DR is evaluated as the ratio between the peak of the THz waveform and the standard deviation of the noise signal when the THz pulse is absent. For this configuration, Fig. 3(b) shows that the maximum DR of 550 is reached for 800 V, whereas higher bias voltages have the effect of abruptly decreasing the DR. It is worth noting that SSBCD allows us to fully explore the DR trend within a much wider range of bias electric fields. Indeed, the dependence of the DR on the bias field qualitatively follows the model first introduced by Lu and Zhang [23], which, to the best of our knowledge, has not been experimentally verified before. According to Lu's model, the DR of biased coherent detection schemes increases monotonically with the DC field for a noiseless DC source. However, for a real DC source, the static field signal noise increases with the field value and is eventually responsible for the drop of DR when the static field noise dominates over the photomultiplier noise equivalent power. Figure 3(c) shows the corresponding power spectrum of the detected THz pulse for an 800 V bias voltage compared with the spectrum obtained by standard ABCD. We found that SSBCD and ABCD detected bandwidths are comparable (∼10 THz), and they are limited by the duration of the probe pulse. It is worth highlighting that for SSBCD, we employed three orders of magnitude lower average probe power (100 μW) and three times lower bias voltage (800 V), compared to the ABCD technique. For this generation of detectors, we observed a dip in the spectrum with a relatively large width centered around 2.5 THz, which is responsible for the multi-cycle shape of the THz waveform. Such a dip corresponds to the first mode etalon effect within the silica cover layer, as expected when considering a thickness of 30 μm and a silica refractive index of ∼2 at THz frequencies.

Building upon our previous investigation, we designed and tested the second generation of SSBCD devices, which consist of a subwavelength slit biased via two metal electrode fingers, as illustrated in Fig. 1(b), to further improve the detector performance and achieve an unaffected 10-THz-wide spectrum detection. This is possible since etalon resonances within the cover layer are now shifted towards higher frequencies, thus potentially enabling detection up to 25 THz. By comparing the performance of the various structures (see Supplement 1), we found that the design featuring a 3-μm-large gap and 10-μm-wide finger electrodes offers the best performance. For this device, the measured THz waveforms obtained at different bias values (in the range 50–600 V) are illustrated in Fig. 4(a). It is worth noting that all the THz waveforms show the same shape. Moreover, the detected signal linearly increases with the bias voltage up to 500 V [Fig. 4(b)], and a drop occurs for 600 V, similarly to what was observed with the first-generation device. Here, the maximum applicable bias was limited by discharge in the air immediately above the cover layer when approaching a voltage of 650 V. Figure 4(b) shows that the best performance, in terms of DR, is achieved for a 300 V bias voltage. Such DR value (∼1200) is more than twice that obtained in the first-generation device, and it is very close to the value recorded for ABCD (∼1300). We relate

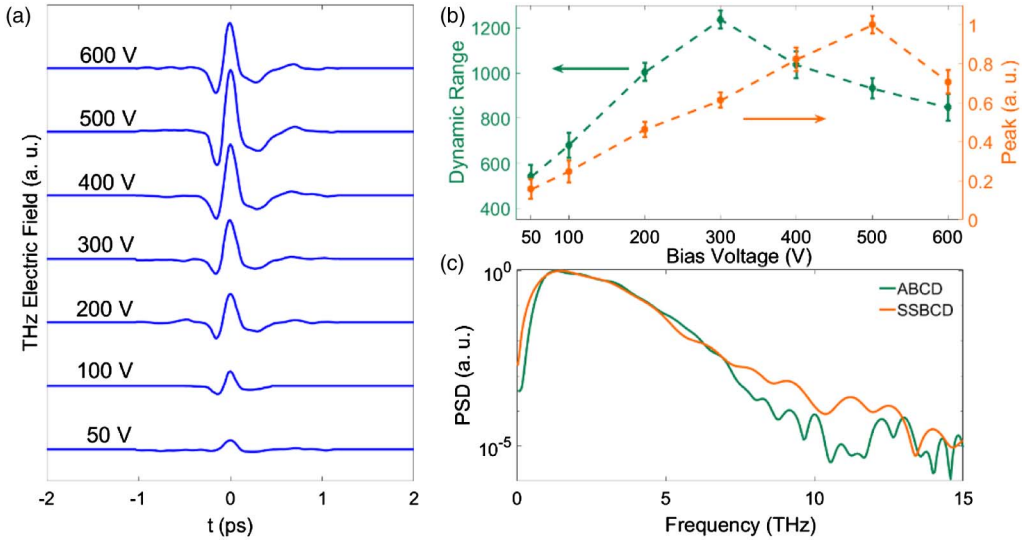

Fig. 4. (a) THz electric field transients recorded via the 3-μm-gap, 10-μm-wide finger detector as a function of the bias voltage. For clarity, the curves are again shifted along the *y* axis. (b) Corresponding dynamic range (dashed green line) and peak signal (dashed orange line) trends as a function of the bias voltage. (c) Power Spectral Density (PSD) evaluated via FFT of the THz waveform at 300 V: comparison between the standard ABCD technique (solid orange line) and detection via our subwavelength slit (SSBCD) device (solid green line).

this improvement to the stronger localization of both the bias and the THz electric fields between the electrodes, resulting in a more efficient interaction in the few-micrometer-long layer of silica. We underline that the SSBCD device in the configuration of 3-μm-gap, 10-μm-finger requires less than half of the bias voltage needed for the optimal operation of the 30-μm-slit when using the same probe power, i.e., 100 μW. Figure 4(c) demonstrates that we achieved a uniform, i.e., gapless, detection bandwidth as wide as that acquired by our implementation of the standard ABCD technique.

Furthermore, as a proof of the ultra-broadband detection capability allowed by the SSBCD method, we performed a spectroscopic investigation on a 1.3-mm-thick pellet of ibuprofen (>98%, Sigma-Aldrich). The pellet was placed at the focus of the THz beam. We recorded both the reference signal (in nitrogen) and the transmitted signal through the sample, and calculated the ratio of the two power spectra, obtaining the transmission curve reported in Fig. 5. Typical spectral features due to vibrational modes of the crystalline structure of ibuprofen are easily recognized in the range 0.6–9.0 THz [24], as also confirmed through the measurement carried out by means of a traditional Fourier-transform spectroscopy (FTS) method.

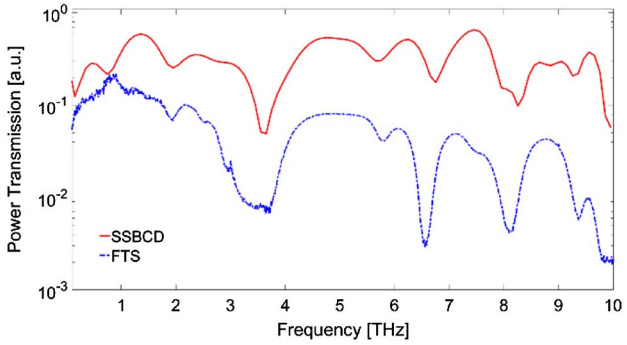

Fig. 5. Transmission spectra for a 1.3-mm-thick pellet of ibuprofen retrieved via SSBCD (red solid curve) and for a 0.6-mm-thick pellet via FTS (blue dashed curve). Curves are shifted along the *y* axis for clarity.

3. CONCLUSION

In conclusion, we demonstrated the first integrated solid-state device for the ultra-broadband coherent detection of THz pulses. SSBCD is featured by relatively high DR (>1200), broad bandwidth (10 THz, limited by the optical pulse duration), and by both a significantly low probe energy (100 nJ) and bias voltages (300 V) with respect to standard ABCD. Our device can be employed as an integrated sensor to fully characterize the whole spectral emission of different THz sources, without the drawbacks associated with conventional band-limited THz detectors. We remark that we are already able to record THz waveforms using bias voltages as low as 50 V, with DR > 500. We also envisage that future optimization of the proposed detector will allow operating the SSBCD with the even lower bias voltages typically provided by common wall plugs, which can be modulated at much higher frequencies and with laser pulses of nanojoule (nJ) energy levels, such as those generated by high-repetition-rate ultrafast lasers (<10 MHz). Incidentally, such types of lasers are routinely employed to feed either large-aperture photoconductive antennas or organic crystals (DAST and DSTMS) generating broadband THz pulses with high conversion efficiencies, which perfectly fit the proposed detection method, e.g., for spectroscopy. Moreover, due to its realization via a simple CMOS-compatible planar technology, SSBCD may lead to a number of advanced yet cost-effective THz devices and instruments, such as novel cameras, where it will be possible to retrieve the full THz waveform in each pixel.

Funding. Natural Sciences and Engineering Research Council of Canada (NSERC) (501100000038); Fonds de Recherche du Québec - Nature et Technologies (FRQNT) (501100003150); Canada Research Chairs; Engineering and Physical Sciences

Research Council (EPSRC) (EP/P51133X/1, EP/P009697/1, EP/M013294/1); Ministère de l'Économie, de la Science et de l'Innovation (MESI) of Québec; Marie Curie Action KOHERENT (299522); Marie Curie Action MC-CIG THEIA (630833); European Union's Horizon 2020 Research and Innovation Programme (725046); 1000 Talents Sichuan Program (China); ITMO Fellowship and Professorship Program (074-U01); Mitacs Accelerate Program (501100004489); Mitacs Elevate Program.

Underlying data relevant to this article can be accessed at Ref. [25].

See Supplement 1 for supporting content.

REFERENCES

1. M. Tonouchi, "Cutting-edge terahertz technology," Nat. Photonics **1**, 97–105 (2007).
2. Y.-S. Lee, *Principles of Terahertz Science and Technology* (Springer, 2009).
3. P. H. Siegel, "Terahertz technology," IEEE Trans. Microwave Theory Tech. **50**, 910–928 (2002).
4. C. Zandonella, "Terahertz imaging: T-ray specs," Nature **424**, 721–722 (2003).
5. B. Ferguson and X. C. Zhang, "Materials for terahertz science and technology," Nat. Mater. **1**, 26–33 (2002).
6. D. Dragoman and M. Dragoman, "Terahertz fields and applications," Prog. Quantum Electron. **28**, 1–66 (2004).
7. A. Ibrahim, D. Ferachou, G. Sharma, K. Singh, M. Kirouac-Turmel, and T. Ozaki, "Ultra-high dynamic range electro-optic sampling for detecting millimetre and sub-millimeter radiation," Sci. Rep. **6**, 23107 (2016).
8. M. Tani, S. Matsuura, K. Sakai, and S. Nakashima, "Emission characteristics of photoconductive antennas based on low-temperature-grown GaAs and semi-insulating GaAs," Appl. Opt. **36**, 7853–7859 (1997).
9. Y. Zhang, X. Zhang, S. Li, J. Gu, Y. Li, Z. Tian, C. Ouyang, M. He, J. Huan, and W. Zhang, "A broadband THz-TDS system based on DSTMS emitter and LTG InGaAs/InAlAs photoconductive antenna detector," Sci. Rep. **6**, 26949 (2016).
10. Q. Wu and X. C. Zhang, "Free-space electro-optic sampling of terahertz beams," Appl. Phys. Lett. **67**, 3523–3525 (1995).
11. A. Tomasino, A. Parisi, S. Stivala, P. Livreri, A. C. Cino, A. C. Busacca, M. Peccianti, and R. Morandotti, "Wideband THz time domain spectroscopy based on optical rectification and electro-optic sampling," Sci. Rep. **3**, 3116 (2013).
12. A. Nahata and T. F. Heinz, "Detection of freely propagating terahertz radiation by use of optical second-harmonic generation," Opt. Lett. **23**, 67–69 (1998).
13. D. J. Cook, J. X. Chen, E. A. Morlino, and R. M. Hochstrasser, "Terahertz-field-induced second-harmonic generation measurements of liquid dynamics," Chem. Phys. Lett. **309**, 221–228 (1999).
14. J. Dai, X. Xu, and X. C. Zhang, "Detection of broadband terahertz waves with a laser-induced plasma in gases," Phys. Rev. Lett. **97**, 103903 (2006).
15. C.-Y. Li, D. V. Seletskiy, Z. Yang, and M. Sheik-Bahae, "Broadband field-resolved terahertz detection via laser induced air plasma with controlled optical bias," Opt. Express **23**, 11436–11443 (2015).
16. N. Karpowicz, J. Dai, X. Lu, Y. Chen, M. Yamaguchi, H. Zhao, and X. C. Zhang, "Coherent heterodyne time-domain spectrometry covering the entire "terahertz gap"," Appl. Phys. Lett. **92**, 011131 (2008).
17. J. Dai, J. Liu, and X. C. Zhang, "Terahertz wave air photonics: terahertz wave generation and detection with laser-induced gas plasma," IEEE J. Sel. Top. Quantum Electron. **17**, 183–190 (2011).
18. U. Gubler and C. Bosshard, "Optical third-harmonic generation of fused silica in gas atmosphere: absolute value of the third-order nonlinear optical susceptibility $\chi^{(3)}$," Phys. Rev. B **61**, 10702–10710 (2000).
19. G. S. May and M. J. Sze, *Fundamentals of Semiconductor Fabrication* (Wiley, 2004).
20. M. Clerici, M. Peccianti, B. E. Schmidt, L. Caspani, M. Shalaby, M. Giguere, A. Lotti, A. Couairon, F. Legare, T. Ozaki, D. Faccio, and R. Morandotti, "Wavelength scaling of terahertz generation by gas ionization," Phys. Rev. Lett. **110**, 253901 (2013).
21. M. Naftaly and R. Dudley, "Methodologies for determining the dynamic ranges and signal-to-noise ratios of terahertz timedomain spectrometers," Opt. Lett. **34**, 1213–1215 (2009).
22. E. Harari, "Dielectric breakdown in electrically stressed thin films of thermal SiO_2," J. Appl. Phys. **49**, 2478–2489 (1978).
23. X. Lu and X. C. Zhang, "Investigation of ultra-broadband terahertz time-domain spectroscopy with terahertz wave gas photonics," Front. Optoelectron. **7**, 121–155 (2014).
24. K. J. Kaltenecker, S. Engelbrecht, K. Iwaszczuk, B. M. Fischer, and P. U. Jepsen, "Ultrabroadband THz time-domain spectroscopy of biomolecular crystals," in *41st International Conference on Infrared, Millimeter, and Terahertz waves (IRMMW-THz)* (2016).
25. All data relevant to this article is accessible at http://dx.doi.org/10.5525/gla.researchdata.462.